JACS JOURNAL OF THE AMERICAN CHEMICAL SOCIETY

Article

Cite This: J. Am. Chem. Soc. 2017, 139, 15494-15503

pubs.acs.org/JACS

Quantum Chemical Modeling of Cycloaddition Reaction in a Self-Assembled Capsule

Henrik Daver,[†] Jeremy N. Harvey,[‡] Julius Rebek, Jr.,[§,∥] and Fahmi Himo*[,†]

[†]Department of Organic Chemistry, Arrhenius Laboratory, Stockholm University, SE-106 91 Stockholm, Sweden

[‡]Department of Chemistry, KU Leuven, Celestijnenlaan 200F, B-3001 Heverlee, Belgium

[§]The Skaggs Institute for Chemical Biology and Department of Chemistry, The Scripps Research Institute, 10550 North Torrey Pines Road, La Jolla, California 92037, United States

[∥]Center for Supramolecular Chemistry and Catalysis, Shanghai University, Shanghai 200444, China

Supporting Information

ABSTRACT: Dispersion-corrected density functional theory is used to study the cycloaddition reaction between phenyl acetylene and phenyl azide inside a synthetic, self-assembled capsule. The capsule is first characterized computationally and a previously unrecognized structure is identified as being the most stable. Next, an examination of the free energies of host–guest complexes is conducted, considering all possible reagent, solvent, and solvent impurity combinations as guests. The experimentally observed relative stabilities of host–guest complexes are quite well reproduced, when the experimental concentrations are taken into account. Experimentally, the presence of the host capsule has been shown to accelerate the cycloaddition reaction and to yield exclusively the 1,4-regioisomer product. Both these observations are reproduced by the calculations. A detailed energy decomposition analysis shows that reduction of the entropic cost of bringing together the reactants along with a geometric destabilization of the reactant supercomplex are the major contributors to the rate acceleration compared to the background reaction. Finally, a sensitivity analysis is conducted to assess the stability of the results with respect to the choice of methodology.

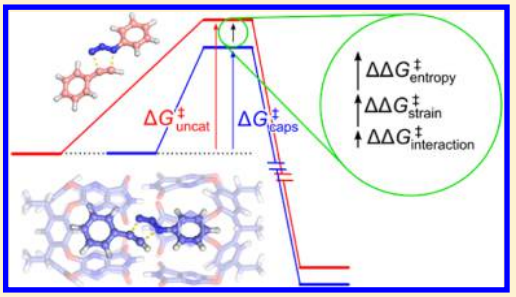

1. INTRODUCTION

With the advent of nanosized container molecules in the 1980s, the possibility to study reactions inside confined spaces arose. A wide variety of reactions have been observed in such molecular chambers.[1−5] Reactants are brought together within the container, screened from interactions with the solvent, and can be prearranged for the reaction. The presence of the capsule can lead to an increase of the reaction rate, and the system can even become catalytic.[6−8]

One specific example of a reaction occurring in a confined space is the cycloaddition of phenyl acetylene **1** and phenyl azide **2** (a "click reaction"), that was observed in the presence of resorcinarene-based host $\mathbf{3}_2$ in deuterated mesitylene solvent, as shown in Scheme 1.[9] The host consists of two vase-shaped resorcinarene-based monomers **3** that are hydrogen-bonded to each other at the rim of the vase units. It was observed that the reaction is accelerated in the presence of the host. Furthermore, only the host-bound 1,4-triazole complex $\mathbf{4}@\mathbf{3}_2$ is formed, while in the absence of $\mathbf{3}_2$, both product regioisomers **4** and **5** are formed in approximately equal amounts.[9] It was suggested that the increased concentration of substrates inside the capsule compared to outside is the source of the acceleration.[9]

The aim of the current study is to investigate how the presence of the capsule affects the free energy profile for this cycloaddition reaction. To this end, we use quantum chemical methodology in the form of dispersion-corrected density functional theory (DFT) to optimize the geometries of all stationary points and transition states along the reaction pathway. Calculating the corresponding energies, a free energy profile for the reaction is obtained and the free energy barrier $\Delta G^{\ddagger}$ for the reaction can be determined. The characterization of the reaction mechanism also includes an assessment of the most stable host–guest complex and the resting state of the reaction. Therefore, all possible complexes with the capsule and the cycloaddition reactants, as well as other compounds present in the solution (Scheme 1c), are taken into consideration.

An implicit aim of the investigation is to assess the adopted quantum chemical approach for studying supramolecular binding free energies and reactions in confined spaces. An overview of cases where quantum chemical methods have been used to calculate supramolecular binding thermodynamics is given in ref 10. In general, only a few theoretical studies of catalysis or rate acceleration within supramolecular host–guest complexes have been reported. Examples include (1) Diels–Alder reactions inside β-cyclodextrin (β-CD)[11−13] and in the so-called "softball" complex,[14] (2) decarboxylation, ester hydrolysis and nucleophilic substitution inside β-CD,[15−17]

Received: August 26, 2017
Published: October 11, 2017

DOI: 10.1021/jacs.7b09102
J. Am. Chem. Soc. 2017, 139, 15494−15503

Scheme 1. Phenyl Acetylene 1 and Phenyl Azide 2 Reacting in Mesitylene-d_{12} (6) in the Absence (a) and Presence (b) of Cavitand 3;[a] (c) Other Possible Capsule Guests

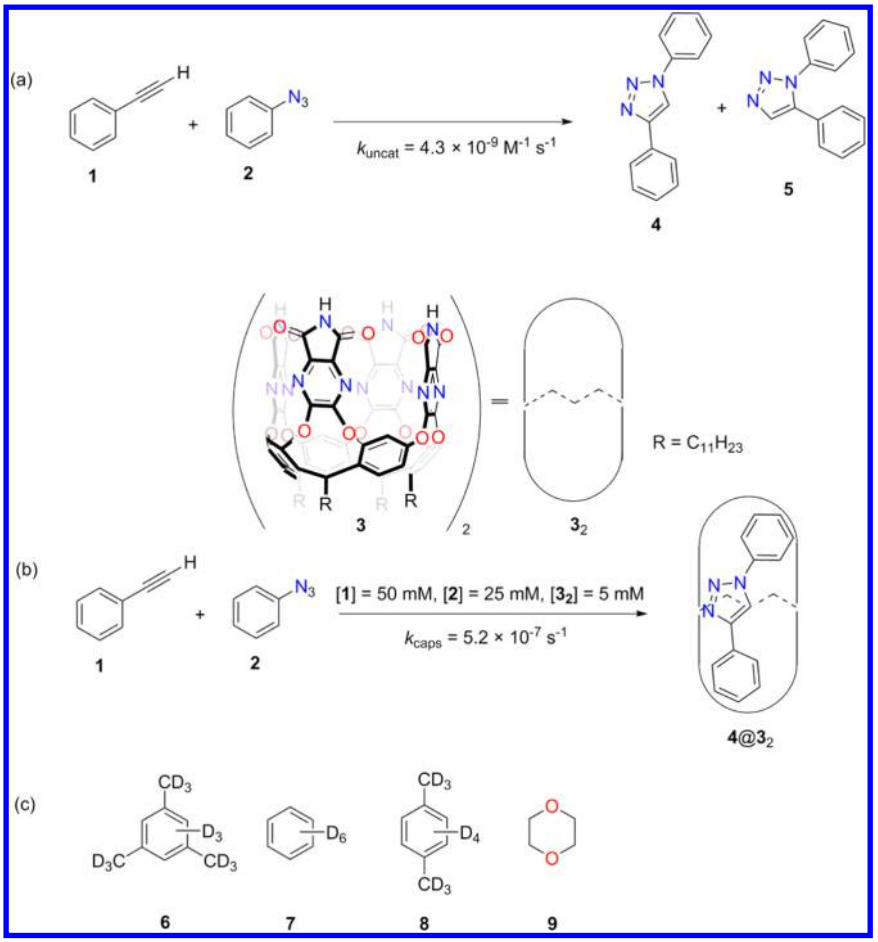

[a]Rate constants are obtained from refs 9 and 20.

and (3) orthoformate hydrolysis and aza-Cope rearrangement inside Raymond's Ga_4L_6 complex.[18,19]

Two previous theoretical studies of 1,3-dipolar cycloaddition reactions in guest−host systems are of interest for the current study. In the first, the reaction between azidoethylamine and propargylamine was studied inside a cucurbit[6]uril by means of DFT calculations.[21,22] The second is concerned with the specific reaction in Scheme 1, which was studied with the ONIOM approach.[23] The capsule was treated at the semi-empirical PM6 level, while the reaction inside was treated with the M06-2X functional.

In the present study, an all-QM methodology is applied for the host−guest system in Scheme 1, taking into account both thermal and solvation effects, which were not included in the previous work.[23] An analysis of the binding thermodynamics of the different guests to the capsule is also carried out, and all computational results are compared to experiments.

2. COMPUTATIONAL DETAILS

All calculations were performed using the B3LYP-D3(BJ) functional[24−30] as implemented in the Gaussian 09 software suite.[31] That is, the B3LYP functional is appended with the two-body terms of the DFT-D3 correction,[28] using the Becke−Johnson damping function.[29,30] B3LYP-D3(BJ) performed among the best functionals in a recent extensive benchmark of reaction barriers for pericyclic reactions.[32]

Geometry optimizations were performed with the 6-31G(d,p) basis set. A thorough conformational search was conducted for each stationary point in order to identify the most stable geometry. This was performed by manually constructing a number of possible starting structures, including different plausible rotamers, hydrogen bonding patterns and binding modes. On the basis of the optimized geometries, single-point calculations were performed with the 6-311+G(2d,2p) basis set. Three-body DFT-D3 dispersion corrections,[28] which are not included in the implementation of B3LYP-D3(BJ) in Gaussian 09, were added separately to these values. In this case, they contributed by up to 6 kcal/mol when the energies of the host−guest complexes were compared to monomer complexes of **3** or to complexes of $\mathbf{3}_2$ without guests bound.

Solvation effects at 298.15 K were calculated with the COSMO*therm* software,[33,34] at the BP86/TZVP level of theory[25,35,36] and with deuterated mesitylene **6** as solvent. To correct for thermal effects at the same temperature, free energy corrections were calculated at the same level of theory as the geometry optimizations. The quasi-rigid-rotor-harmonic-oscillator (quasi-RRHO) approach was used, which includes a correction for the erroneous asymptotic dependence on low-frequency vibrations in the standard RRHO approach.[37] The quasi-RRHO calculations were done with symmetry numbers σ_r = 1. For compounds with higher symmetry, the term (RT ln σ_r) was added to the free energies.

The free energy corrections are calculated in the 1 atm standard state, while the reference state in solution is the 1 M state for all compounds except the solvent, which has a concentration of 7.2 M. To correct for this, the correction term RT ln(1/24.5 L/mol × 1 mol/L) = 1.9 kcal/mol was added to all compounds except mesitylene, for

DOI: 10.1021/jacs.7b09102
J. Am. Chem. Soc. 2017, 139, 15494−15503

which the correction term RT ln(1/24.5 L/mol × 7.2 mol/L) = 3.1 kcal/mol was added.

To calculate the fraction of the inner volumes of hosts that are occupied by guests, i.e., the so-called packing coefficients (PCs) of the host–guest complexes,[38] the VOIDOO software[39] was used to calculate the van der Waals volumes of the guests and to identify cavities inside the hosts. The cavity volumes were then determined using a variant of the cavity-filling method,[38] as described in detail in Supporting Information. Bondi atomic radii[40] were used in these volume calculations.

Finally, several tests were made to probe the sensitivity of the results with respect to the chosen computational protocol. The results of these tests are summarized in Section 3.5 below.

3. RESULTS AND DISCUSSION

The results are organized as follows: First, the capsule is characterized in mesitylene-d_{12} (**6**), with and without **6** and/or the solvent impurities benzene-d_6 (**7**) and *p*-xylene-d_{10} (**8**) bound. Next, acetylene **1**, azide **2** and dioxane **9**, an impurity in the commercial solution of **1**, are introduced and the calculated relative free energies of the different complexes are evaluated. The uncatalyzed cycloaddition reaction is then characterized, before studying the cycloaddition of **1** and **2** inside $\mathbf{3}_2$. The calculated binding free energies and barriers are compared to experimental observations, as well as to the results obtained in the previous computational study of the same reaction.[23] Finally, the sensitivity of the results to the choice of some aspects of the computational methodology will be assessed.

3.1. Characterization of Capsule. Experimentally, in off-the-shelf solvent **6**, the NMR signals revealed a complex between $\mathbf{3}_2$ and the solvent impurities **7** and **8**.[41] It was argued that these two guests make a better fit to the capsule than, for example, two molecules of **6** would.[41] The **3** unit of the complex was observed to be of approximate C_{4v} symmetry, so the dimer structure is therefore termed $(\mathbf{3}\text{-}C_{4v})_2$. The overall symmetry of the cavitand dimer, without guests, is approximately D_{4d}.

In the current study, a computational model of **3** is used in which the undecyl substituents on the cavitands were replaced with methyl groups. When the geometry of the corresponding complex between $(\mathbf{3}\text{-}C_{4v})_2$ and **7** and **8** was optimized, the guests were found to arrange inside the capsule in a diagonal manner, such that the phenyl rings avoid steric repulsion with the pyrazine units of the cavitands. The geometry of this complex, called $\mathbf{7}\cdot\mathbf{8}@(\mathbf{3}\text{-}C_{4v})_2$, is given in Figure 1.

In this structure, the N–H groups at the rim of each **3** unit form bifurcated hydrogen bonds to two carbonyl oxygens in the other **3** unit, so in total eight bifurcated hydrogen bonds are formed between the monomers, with an average NH···O hydrogen bond distance of 2.12 Å. The inner volume of $(\mathbf{3}\text{-}C_{4v})_2$ is calculated to be 462 Å^3, and the packing coefficient of **7** and **8** is calculated to be 0.43.

However, several imaginary frequencies were obtained when a vibrational analysis was carried out for the $\mathbf{7}\cdot\mathbf{8}@(\mathbf{3}\text{-}C_{4v})_2$ complex. Upon further optimization the hydrogen bonds along the seam of the cavitand dimer reorganized and a new structure was found for the capsule in which each pyrazine-imide unit has twisted slightly such that the monomers now are close to adopting C_4 symmetry (see Figure 1). The calculations show this to be the most stable conformation of $\mathbf{3}_2$, and hence the complex with **7** and **8** is simply named $\mathbf{7}\cdot\mathbf{8}@\mathbf{3}_2$. The cavitand dimer in this complex is of approximate S_8 symmetry. One carbonyl oxygen of each imide unit now points out toward the solvent, while the other carbonyl accepts a hydrogen bond from

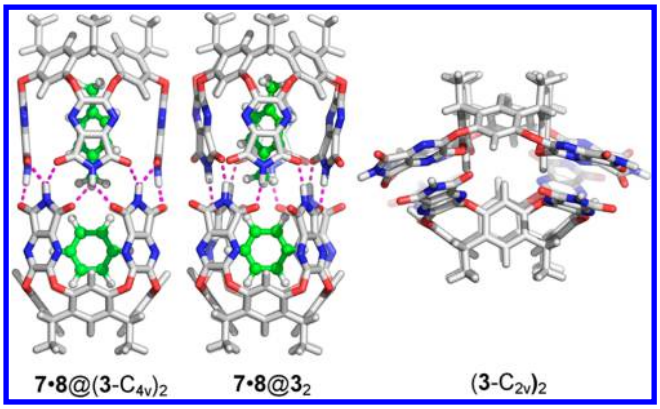

Figure 1. Optimized structures of the encapsulation complexes of **7** and **8** with cavitands of C_{4v} (left) and C_4 (middle) symmetry. The velcrand dimer, composed of C_{2v}-symmetric kite-shaped resorcinarenes, is shown to the right for comparison.

an NH group at the rim of the complementary **3** unit in the complex. Like in the case of the C_{4v} structure, the total number of hydrogen bonds in the structure is eight, but the more linear arrangement of donors and acceptors in the C_4 structure results in shorter hydrogen bonds—the average NH···O hydrogen bond distance is 1.80 Å.

Complex $\mathbf{7}\cdot\mathbf{8}@\mathbf{3}_2$ is calculated to be as much as 12.1 kcal/mol more stable than $\mathbf{7}\cdot\mathbf{8}@(\mathbf{3}\text{-}C_{4v})_2$.[42] Importantly, inclusion of the dispersion corrections has a considerable effect here. If neglected, the C_{4v} structure is calculated to be 4.9 kcal/mol more stable than the C_4 one, i.e., the effect of the dispersion correction is as much as 17 kcal/mol on the relative energy.

In the experiments, the signals observed in the NMR measurements correspond to a complex with C_{4v}-symmetric cavitands.[41,43] The computational result that the C_4 species is the more stable one might at first seem inconsistent with this observation. However, there are two isomers of the C_4-symmetric cavitands, in which different carbonyl oxygens are exposed to the solvent. These isomers can interconvert via the C_{4v} structure. Using transition state theory (TST), an energy barrier of 12.1 kcal/mol can be converted to a rate constant of about 9000 s^{-1}. This value is a lower bound for the rate of interconversion of the isomers, since there might be a lower-energy transition state (TS) that involves local motions of each pyrazine-imide unit. Hence, a reasonable suggestion is that the cavitands in the $\mathbf{7}\cdot\mathbf{8}@\mathbf{3}_2$ complex rapidly convert between the two C_4 isomers, giving rise to a time-averaged C_{4v}-type NMR signal.

Interestingly, the C_4 capsule is calculated to have a considerably smaller inner volume than the C_{4v} one, 379 vs 462 Å^3. Compared to the empty $\mathbf{3}_2$, the packing coefficient of **7** and **8** is now calculated to be 0.57, which is thus closer to the value of 0.55 proposed to be optimal in similar inclusion complexes.[38]

Experimentally, when $\mathbf{3}_2$ was added to a distilled solution of **6**, i.e., without impurities **7** or **8** present, a broad ^{1}H NMR spectrum was obtained, making it hard to characterize which complexes are formed.[41] Upon comparison to the spectra obtained in other solvents it was concluded that the mesitylene-filled capsule complex $\mathbf{6}\cdot\mathbf{6}@\mathbf{3}_2$ is not the one preferentially formed.[41] In the calculations, when the geometry of $\mathbf{6}\cdot\mathbf{6}@\mathbf{3}_2$ was optimized, several hydrogen bonds were broken and the symmetry of the capsule was lost. This complex is calculated to be 11.4 kcal/mol higher in energy compared to $\mathbf{7}\cdot\mathbf{8}@\mathbf{3}_2$.

DOI: 10.1021/jacs.7b09102
J. Am. Chem. Soc. 2017, 139, 15494–15503

The calculations suggest that the most stable form of **3** in absence of guests is the dimer of C_{2v}-symmetric cavitands, termed $(\mathbf{3}\text{-}C_{2v})_2$ (Figure 1). This complex has previously been referred to as a "kite" or "velcrand" structure[43,44] and has an overall D_{2d} symmetry. Experimentally, when **7** and **8** were added in excess to a solution of $\mathbf{3}_2$ in distilled **6**, a sharp signal corresponding to $\mathbf{7}\cdot\mathbf{8}@\mathbf{3}_2$ was observed.[41] This means that eq 1 must be endergonic.

$$\mathbf{7}\cdot\mathbf{8}@\mathbf{3}_2 \rightleftharpoons (\mathbf{3}\text{-}C_{2v})_2 + \mathbf{7} + \mathbf{8} \quad (1)$$

Consistently with this observation, the free energy of separate **7**, **8** and $(\mathbf{3}\text{-}C_{2v})_2$ is calculated to be +5.7 kcal/mol relative to $\mathbf{7}\cdot\mathbf{8}@\mathbf{3}_2$. It should be noted here that the relative stability of the kite structure $(\mathbf{3}\text{-}C_{2v})_2$ with respect to $\mathbf{7}\cdot\mathbf{8}@\mathbf{3}_2$ is somewhat sensitive to the choice of computational methodology, as will be discussed in Section 3.5 below.

In summary, in the absence of guests, the most stable conformer of **3** is calculated to be the kite-dimeric complex $(\mathbf{3}\text{-}C_{2v})_2$. With guests present, a previously unrecognized approximately C_4-symmetric geometry for the cavitands is identified as the most stable complex $\mathbf{7}\cdot\mathbf{8}@\mathbf{3}_2$. This structure is maintained also when other guests bind inside the host, which will be discussed in the following section.

3.2. Binding Free Energies of Various Species. The calculated free energies of all possible complexes formed in the presence of solvent **6**, benzene **7**, and xylene **8** are listed in Table 1. We first note that the monomeric complexes (Table 1, entries 3–6) are all calculated to be considerably less stable than the dimeric ones.

Table 1. Calculated Free Energies (kcal/mol), Relative to $\mathbf{7}\cdot\mathbf{8}@\mathbf{3}_2$, and Packing Coefficients of Different Host–Guest Complexes

entry	complex	$\Delta G°$	packing coefficient
1	$(\mathbf{3}\text{-}C_{2v})_2$[a]	+5.7	
2	$\mathbf{3}_2$	+10.9	
3	**2 × 3**	+40.3	
4	**2 × 6@3**[a]	+24.0	
5	**2 × 7@3**	+29.3	
6	**2 × 8@3**	+31.7	
7	$\mathbf{6}\cdot\mathbf{6}@\mathbf{3}_2$	+11.4	0.76
8	$\mathbf{7}\cdot\mathbf{7}@\mathbf{3}_2$	+0.9	0.48
9	$\mathbf{8}\cdot\mathbf{8}@\mathbf{3}_2$	+6.8	0.67
10	$\mathbf{6}\cdot\mathbf{7}@\mathbf{3}_2$	+7.4	0.62
11	$\mathbf{6}\cdot\mathbf{8}@\mathbf{3}_2$[a]	+11.8	0.72
12	$\mathbf{7}\cdot\mathbf{8}@\mathbf{3}_2$	0.0	0.57

[a]Imaginary frequencies <20*i* cm^{-1} were found and treated as real in the quasi-RRHO calculations for these complexes.

The calculated stabilities of the homocapsules $\mathbf{7}\cdot\mathbf{7}@\mathbf{3}_2$ and $\mathbf{8}\cdot\mathbf{8}@\mathbf{3}_2$ relative to the heterocapsule $\mathbf{7}\cdot\mathbf{8}@\mathbf{3}_2$ can be directly compared to experiments as the following guest exchange reactions were studied experimentally:[41]

$$\mathbf{7}\cdot\mathbf{8}@\mathbf{3}_2 + \mathbf{7} \rightleftharpoons \mathbf{7}\cdot\mathbf{7}@\mathbf{3}_2 + \mathbf{8} \quad (2)$$

$$\mathbf{7}\cdot\mathbf{8}@\mathbf{3}_2 + \mathbf{8} \rightleftharpoons \mathbf{8}\cdot\mathbf{8}@\mathbf{3}_2 + \mathbf{7} \quad (3)$$

A 70-fold excess of **7** to **8** was needed to form $\mathbf{7}\cdot\mathbf{7}@\mathbf{3}_2$,[41] which corresponds to eq 2 being endergonic by 2.5 kcal/mol (*RT* ln 70). The calculated free energy for this reaction is +0.9 kcal/mol. Furthermore, the complex $\mathbf{8}\cdot\mathbf{8}@\mathbf{3}_2$ could not be observed at 70-fold excess of **8** to **7**,[41] indicating that eq 3 is endergonic by more than 2.5 kcal/mol. The calculated free energy difference is +6.8 kcal/mol.

When acetylene **1** and azide **2** are added to the solution of $\mathbf{3}_2$ in off-the-shelf **6**, a number of new host–guest complexes are possible. Dioxane **9** is present as a < 1% impurity in the commercial solution of **1** and can also be a part of such complexes. The geometries of all possible new host–guest complexes have been optimized, and the calculated relative free energies of these complexes are listed in Table 2 (optimized geometries of all compounds in Tables 1 and 2 are given in the Supporting Information).

Table 2. Calculated Free Energies (kcal/mol), Relative to $\mathbf{7}\cdot\mathbf{8}@\mathbf{3}_2$, and Packing Coefficients of Different Host–Guest Complexes

entry	complex	$\Delta G°$	$\delta G'$[a]	$\Delta G'$[b]	packing coefficient
1	$\mathbf{1}\cdot\mathbf{1}@\mathbf{3}_2$	+0.5	−2.7	−2.2	0.61
2	$\mathbf{1}\cdot\mathbf{2}@\mathbf{3}_2$	−1.5	−2.3	−3.8	0.61
3	$\mathbf{1}\cdot\mathbf{6}@\mathbf{3}_2$	+8.6	−4.5	+4.1	0.69
4	$\mathbf{1}\cdot\mathbf{7}@\mathbf{3}_2$	−0.6	−1.4	−2.0	0.54
5	$\mathbf{1}\cdot\mathbf{8}@\mathbf{3}_2$	+1.8	−1.4	+0.4	0.64
6	$\mathbf{1}\cdot\mathbf{9}@\mathbf{3}_2$	−1.0	0.0	−1.0	0.55
7	$\mathbf{2}\cdot\mathbf{2}@\mathbf{3}_2$	−3.2	−1.9	−5.1	0.61
8	$\mathbf{2}\cdot\mathbf{6}@\mathbf{3}_2$[c]	+11.1	−4.1	+7.0	0.69
9	$\mathbf{2}\cdot\mathbf{7}@\mathbf{3}_2$	−2.0	−1.0	−3.0	0.55
10	$\mathbf{2}\cdot\mathbf{8}@\mathbf{3}_2$	+2.7	−1.0	+1.7	0.64
11	$\mathbf{2}\cdot\mathbf{9}@\mathbf{3}_2$	−2.7	+0.4	−2.3	0.55
12	$\mathbf{6}\cdot\mathbf{9}@\mathbf{3}_2$	+11.3	−1.8	+9.5	0.63
13	$\mathbf{7}\cdot\mathbf{7}@\mathbf{3}_2$	+0.9	0.0	+0.9	0.48
14	$\mathbf{7}\cdot\mathbf{8}@\mathbf{3}_2$	0.0	0.0	0.0	0.57
15	$\mathbf{7}\cdot\mathbf{9}@\mathbf{3}_2$	+3.1	+1.4	+4.5	0.48
16	$\mathbf{8}\cdot\mathbf{8}@\mathbf{3}_2$	+6.8	0.0	+6.8	0.67
17	$\mathbf{8}\cdot\mathbf{9}@\mathbf{3}_2$	+0.2	+1.4	+1.6	0.58
18	$\mathbf{9}\cdot\mathbf{9}@\mathbf{3}_2$[c]	−1.8	+2.7	+0.9	0.49

[a]$\delta G' = RT \ln([\text{guest 1}][\text{guest 2}]/[\mathbf{7}][\mathbf{8}])$. Calculated at [**1**] = 50 mM, [**2**] = 25 mM, [**6**] = 7.2 M, [**7**] = [**8**] = 5 mM, and [**9**] = 0.5 mM. [b]$\Delta G' = \Delta G° + \delta G'$. [c]For these complexes, imaginary frequencies <20*i* cm^{-1} were found and treated as real in the quasi-RRHO calculations.

Experimentally, five capsule complexes were observed in the NMR, in the following order of abundance: $\mathbf{1}\cdot\mathbf{2}@\mathbf{3}_2 > \mathbf{2}\cdot\mathbf{9}@\mathbf{3}_2 > \mathbf{2}\cdot\mathbf{2}@\mathbf{3}_2 > \mathbf{1}\cdot\mathbf{1}@\mathbf{3}_2 > \mathbf{1}\cdot\mathbf{9}@\mathbf{3}_2$.[9] With the exception of $\mathbf{1}\cdot\mathbf{1}@\mathbf{3}_2$, all of these complexes are calculated to be more stable than $\mathbf{7}\cdot\mathbf{8}@\mathbf{3}_2$ under 1 M concentrations. Also formation of complexes $\mathbf{1}\cdot\mathbf{7}@\mathbf{3}_2$, $\mathbf{2}\cdot\mathbf{7}@\mathbf{3}_2$ and $\mathbf{9}\cdot\mathbf{9}@\mathbf{3}_2$ were calculated to be favorable.

The packing coefficients listed in Table 1 and 2 are the ratios of the van der Waals volumes of the guests to the inner volume of the (fictitious) empty $\mathbf{3}_2$ complex (350 $Å^3$). The complexes with packing coefficients between 0.48 and 0.61 are found to be within 3 kcal/mol in free energy relative to $\mathbf{7}\cdot\mathbf{8}@\mathbf{3}_2$, while complexes with larger coefficients are overall less stable. This is in good agreement with the 55% rule for optimal occupancy in similar inclusion complexes.[38] Optimized geometries and calculated guest volumes for all host–guest complexes are given in Supporting Information.

In order to assess how the concentration of the guests affects the relative abundance of inclusion complexes, the term $\delta G' = RT \ln([\text{guest 1}][\text{guest 2}]/[\mathbf{7}][\mathbf{8}])$ is introduced for the transformation from the standard state used in the calculations (1 M concentrations for solutes, 7.2 M for **6**) to the experimental conditions (that is, [**1**] = 50 mM, [**2**] = 25

DOI: 10.1021/jacs.7b09102
J. Am. Chem. Soc. 2017, 139, 15494–15503

mM, [**6**] = 7.2 M, [**7**] and [**8**] were set to 5 mM, and [**9**] was set to 0.5 mM).[9]

Under these conditions, the driving force for binding **1** and **2** is larger than above, while **9** is less preferentially bound (Table 2). The stability order of complexes is calculated to be **2·2**@3_2 > **1·2**@3_2 > **2·7**@3_2 > **2·9**@3_2 > **1·1**@3_2 > **1·7**@3_2 > **1·9**@3_2. Compared to the experimental order (vide supra) two differences are noted: The predicted benzene complexes **1·7**@3_2 and **2·7**@3_2 are not observed experimentally, and the calculated stability of **2·2**@3_2 is overestimated compared to **1·2**@3_2 and **2·9**@3_2.

Experimentally, the **1·2**@3_2 complex was found to be the most abundant species, and an equilibrium constant $K_D = 9 \pm 3$ was measured for the disproportionation eq 4, corresponding to a reaction exergonicity of 1.3 ± 0.2 kcal/mol.[9]

$$\mathbf{1{\cdot}1}@3_2 + \mathbf{2{\cdot}2}@3_2 \rightleftharpoons 2 \times \mathbf{1{\cdot}2}@3_2 \quad (4)$$

In the calculations, the free energy of this reaction is −0.4 kcal/mol including the concentration correction, in reasonable agreement with the experimental value. The structures of these three complexes are shown in Figure 2.

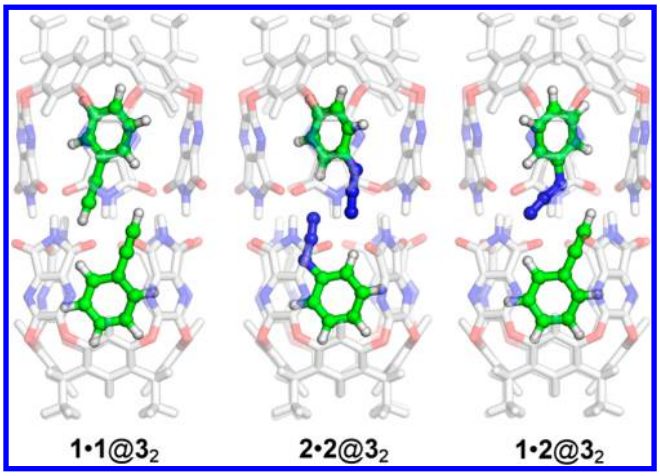

Figure 2. Optimized geometries of the homo- and heterocapsule complexes with the guests **1** and **2**. The capsule is made transparent for clarity.

3.3. Cycloaddition in Absence of Capsule. It is of interest to first characterize the cycloaddition reaction occurring in the absence of capsule, in order to assess the geometric and energetic influence of the capsule on the reaction. The uncatalyzed reaction has been studied computationally previously,[23,45] but not at the same level of theory as the one used in the current study.

First, a reactant supercomplex between **1** and **2**, termed **1·2**, is calculated to be 4.0 kcal/mol higher in free energy than the separated reactants (Figure 3a). In the most stable geometry of this complex, the phenyl rings of the reactants form π-stacking interactions with each other, while the azide and the acetylene moieties are aligned in a way that resembles the 1,5-cycloaddition product **5**. The distances between both the proximal N and C atoms and the distal N and C atoms are ca. 3.3 Å.

The geometries of the two cycloaddition transition states, termed **4-TS** (leading to the 1,4-product) and **5-TS** (leading to the 1,5-product), were optimized and are shown in Figure 3. The two TSs are calculated to be of similar energy relative to the separated reactants: + 28.0 kcal/mol and +26.5 kcal/mol for

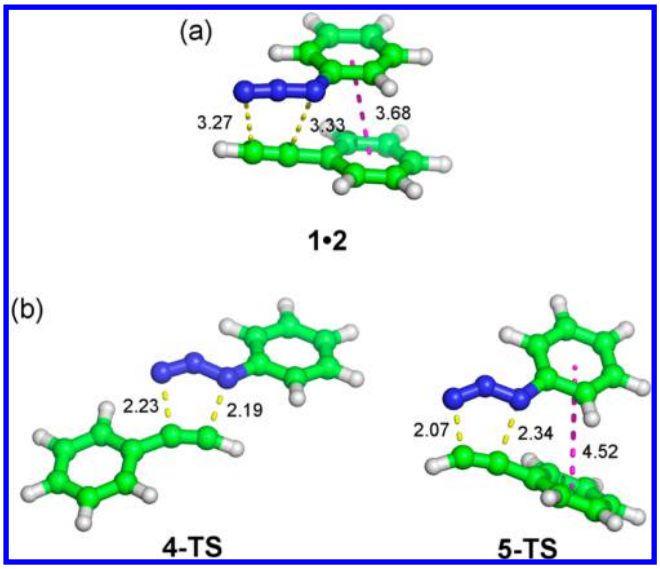

Figure 3. Optimized geometries of (a) the reactant supercomplex and (b) the transition states toward formation of the 1,5- and 1,4-cycloaddition products. Important distances (Å) are indicated.

4-TS and **5-TS**, respectively. Both values are close to the experimental barrier of 29 kcal/mol, as estimated from the measured k_{uncat} value of 4.3×10^{-9} M^{-1} s^{-1}.[9] The optimized geometry of **4-TS** is quite symmetrical with respect to the forming N−C bonds; 2.23 and 2.19 Å for the proximal and distal nitrogens, respectively. The bond formation is calculated to occur in a slightly less synchronous fashion in **5-TS**, where the formation of the bond between the distal nitrogen and carbon is more advanced than the proximal N−C bond (2.07 vs 2.34 Å). In **5-TS**, the phenyl rings are ca. 0.8 Å further apart from each other compared to **1·2**.

Finally, the formation of both products is calculated to be very exergonic, with the 1,4-cycloaddition product being the slightly more stable one (−52.6 kcal/mol and −50.1 kcal/mol relative to the separated reactants for **4** and **5**, respectively).

3.4. Cycloaddition Inside Capsule. As discussed above, complex **1·2**@3_2 was experimentally found to be the most stable host−guest complex.[9] It will therefore be used as the starting-point for the reactivity study here and can be termed as the "Michaelis complex" of the reaction. The calculations predict complex **1·2**@3_2 to be 1.7 kcal/mol higher than **2·2**@3_2, at 1 M standard state. This is a reasonably small error that can be ascribed to the adopted computational methodology.

The arrangement of substrates in 3_2 is in a conformation that is reminiscent of the **4-TS**. Other arrangements of the reactants inside the capsule were also evaluated, but turned out to have higher energies (see SI). The distances from the proximal and distal nitrogens to the respective acetylene carbons are 3.16 and 3.30 Å, respectively. From **1·2**@3_2, the transition state for formation of **4** inside the capsule (**4-TS**@3_2) was optimized, as shown in Figure 4, and is calculated to be 21.6 kcal/mol higher in energy than **1·2**@3_2. In **4-TS**@3_2, the rings of the reactants are found to be more coplanar inside the capsule compared to the same TS in solution. The dihedral angles between phenyl ring and substituent in the TS decrease upon encapsulation, from 32° to 8° for the **1** unit and from 11° to 2° for **2**. The forming N−C bonds are, however, of similar lengths in the reactions regardless of the presence of the capsule.

The energy of the product complex **4**@3_2 was calculated, and the exergonicity of the cycloaddition reaction is found to

DOI: 10.1021/jacs.7b09102
J. Am. Chem. Soc. 2017, 139, 15494−15503

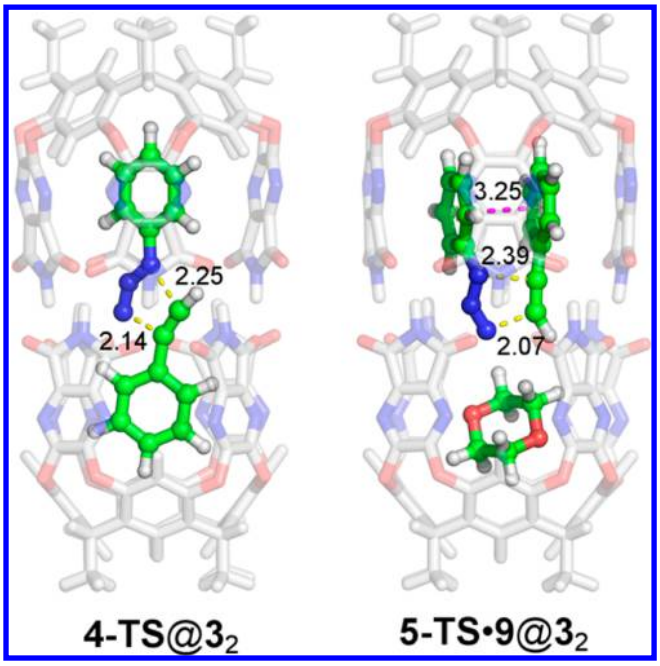

Figure 4. Optimized geometries of encapsulated transition states.

increase somewhat inside the capsule compared to outside. Inside the capsule, the reaction **1**·**2**@3_2 → **4**@3_2 has a calculated exergonicity of 56.8 kcal/mol, while the outside reaction **1** + **2** → **4** is calculated to be exergonic by 52.6 kcal/mol. Interestingly, among the molecules considered, product **4** is calculated to be the best guest to the capsule, predicting product inhibition rather than turnover. Compared to **7**·**8**@3_2, the binding free energy of **4** to 3_2 is calculated to be −5.7 kcal/mol at 1 M concentrations—a larger binding free energy than any of the entries in Table 2. This is in part due to entropic reasons since in **4**@3_2 only one guest molecule is bound, while the entries in Table 2 include two guest molecules.

To perform a second cycloaddition reaction, product **4** must be released from the capsule and new **1** and **2** substrates must bind. The net corresponding reaction, eq 5, is calculated to be endergonic by 4.2 kcal/mol.

$$\mathbf{4}@3_2 + \mathbf{1} + \mathbf{2} \rightleftharpoons \mathbf{1}\cdot\mathbf{2}@3_2 + \mathbf{4} \quad (5)$$

Hence, the barrier for going from the product state **4**@3_2 in one catalytic cycle to the **4-TS**@3_2 transition state in the next cycle is calculated to be 4.2 + 21.6 = 25.8 kcal/mol. The full free energy profiles of the 1,3-cycloaddition giving the 1,4-product **4** in the presence and absence of capsule are shown in Figure 5.

The higher barrier calculated for the second cycle is consistent with the experimental finding that no turnover is observed. Namely, an increase of 4.2 kcal/mol in the reaction barrier corresponds to the reaction rate being decreased ca. 1200-fold. In the experiments, the system was monitored for 6 days in order to observe one single turnover of the system.[9] A 1200 times slower reaction will thus not be observed on the same time scale. It should be noted that the exchange of guests is here assumed to be governed by thermodynamics only, which means that the barriers associated with such processes are assumed to be lower than the barriers for the chemical transformation inside the capsule. Such an assumption is supported by the experimental observation that the distribution of host−guest complexes equilibrate on a time scale of seconds[46] or minutes,[41] which indicates that barriers of less than 20 kcal/mol are involved.

The transition state to form the other regioisomer (**5-TS**·**9**@3_2) was also optimized inside the capsule and the geometry is shown in Figure 4. Interestingly, in this TS, it was found that both substrates are bound in one cavitand unit while the other cavitand hosts a dioxane molecule **9**, which leads to a lower energy compared to the TS without dioxane. The binding of benzene **7** in that position was also examined, i.e., **5-TS**·**7**@3_2, and was found to be 2.1 kcal/mol higher in energy at 1 M concentrations. The diagonal arrangement of substrates in the cavitand seen in **4-TS**@3_2 is broken in favor of π-stacking interactions between the substrates and the pyrazine walls of the capsule. As a result of this, the distance between the phenyl rings is shortened by 1.3 Å compared to the geometry of uncatalyzed **5-TS**. To encompass this bulkier TS, the capsule

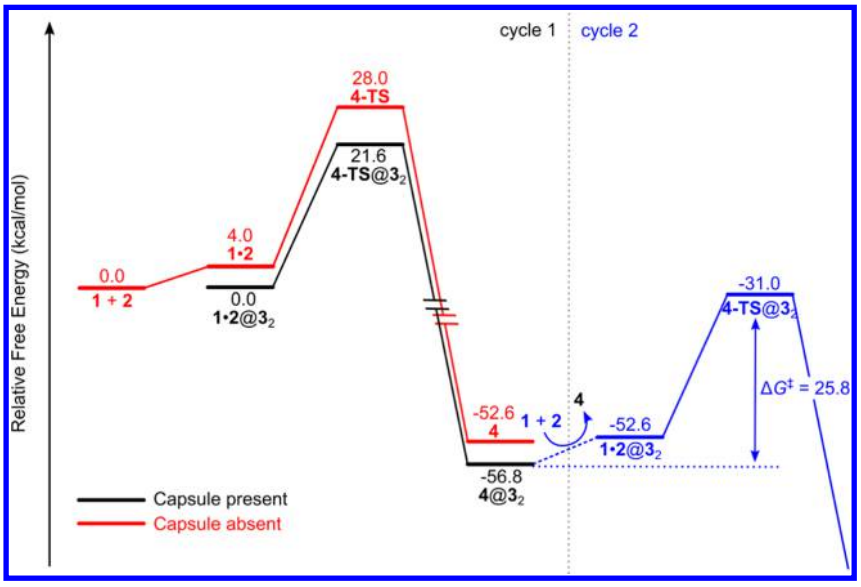

Figure 5. Free energy profiles for the formation of **4** in the presence (black, blue) and absence (red) of capsule.

DOI: 10.1021/jacs.7b09102
J. Am. Chem. Soc. 2017, 139, 15494−15503

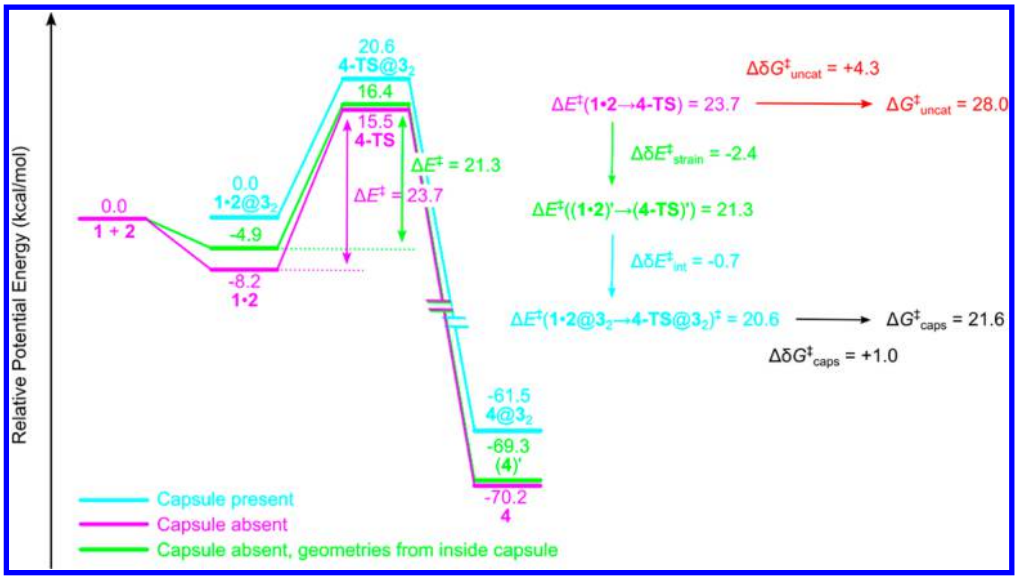

Figure 6. Potential energy profile (i.e., calculated without free energy corrections) for formation of **4** in presence (blue) and absence (magenta, green) of 3_2. An energy decomposition scheme is shown to the right.

has to be widened somewhat, as seen from Figure 4. **5-TS·9@3_2** is calculated to be as much as 18.7 kcal/mol higher in free energy compared to **4-TS@3_2**, and this pathway can be discarded. The capsule raises thus the barrier by 13.8 kcal/mol as compared to the uncatalyzed reaction. In contrast, the reaction barrier involving **4-TS** is lowered from 28.0 kcal/mol outside to 21.6 kcal/mol inside the capsule.

Here, it is informative to compare the calculated reaction barrier to the experimentally measured rate constants. In the presence of the capsule, a k_{caps} value of 5.2×10^{-7} s^{-1} can be derived from the reported values of v_{caps} and K_D.[20] This rate constant can be converted to a free energy barrier of 26 kcal/mol. The calculations thus underestimate the barrier inside the capsule by ca. 4 kcal/mol.

How then does the capsule accelerate the reaction? The catalytic action of the capsule has been suggested to be due to the higher concentration of substrates inside the capsule compared to outside.[9] The concentration of each reactant inside a capsule of 373 Å^3 volume, as was calculated for **1·2@3_2**, becomes 4.5 M. Inserting this value into a bimolecular rate equation, $v_{caps} = k'_{caps} \times (4.5\ M)^2$, and using the value of $v_{caps} = 1.3 \times 10^{-9}$ M s^{-1} from ref 9, yields a rate constant k'_{caps} of 6.4×10^{-11} M^{-1} s^{-1}, which corresponds to a free energy barrier of 31.4 kcal/mol for the cycloaddition, i.e., 2.5 kcal/mol higher than the outside reaction. In contrast, in the current study a significantly lower barrier is calculated in the presence of capsule, and the concentration hypothesis is thus not supported by the calculations. This conclusion is insensitive to the estimation of the inner volume of the capsule. For example, if the volume for **7·8@(3-C_{4v})$_2$** is used, 462 Å^3, the concentration inside becomes 3.6 M, k'_{caps} becomes 1.0×10^{-10} M^{-1} s^{-1}, and the free energy barrier becomes 31.1 kcal/mol.

Another way to catalyze the reaction is to stabilize the TS more than the reactants, leading to a lowering of the barrier. In order to assess the difference in the interactions between the capsule and the reactants vs the transition state, the geometries of the encapsulated species were extracted from the structures of **1·2@3_2** and **4-TS@3_2**, called **(1·2)′** and **(4-TS)′**, and their potential energies (approximately equivalent to enthalpies) were evaluated (blue and green lines in Figure 6). At this level of theory, the barrier from **1·2@3_2** to **4-TS@3_2** is 20.6 kcal/mol. **(4-TS)′** is calculated to be 21.3 kcal/mol higher in energy than **(1·2)′**, so the interactions between host and guests are calculated to stabilize the TS with respect to the reactant supercomplex by only $\Delta\delta E^{\ddagger}_{int}$ = 20.6−21.3 = −0.7 kcal/mol. This shows that the capsule does not provide any significant stabilization of the TS compared to the reactant complex.

On the other hand, an interesting observation that can be made from this analysis is that **(1·2)′** is calculated to be 3.3 kcal/mol higher in energy than **1·2**, while **(4-TS)′** is only 0.9 kcal/mol higher than **4-TS**. This destabilization comes from the geometric strain induced by the encapsulation (vide supra), and the fact that the reactant supercomplex becomes more strained inside the capsule than the transition state leads to a barrier lowering of $\Delta\delta E^{\ddagger}_{strain}$ = −2.4 kcal/mol, contributing thus significantly to the rate acceleration.

Now, consider the optimized geometries of **1·2** and **4-TS** in absence of capsule (with the thermal effects omitted for proper comparison). As shown in the energy profile in Figure 6, **1·2** is calculated to be 8.2 kcal/mol more stable than the separated reactants, **1** + **2**. The barrier from **1·2** to **4-TS** is calculated to be 23.7 kcal/mol. The calculated free energy barrier outside the capsule is 28.0 kcal/mol, which shows that the effect of including the thermal corrections, roughly corresponding to the entropic contributions, is thus $\Delta\delta G^{\ddagger}_{uncat}$ = 28.0−23.7 = −4.3 kcal/mol on the barrier outside the capsule. Inside the capsule, the calculated free energy barrier is 21.6 kcal/mol while the barrier without thermal corrections is 20.6 kcal/mol, resulting in an entropic effect of only 1.0 kcal/mol. This analysis shows that the reduction of the entropic cost of bringing together the reactants (1.0−4.3) = −3.3 kcal/mol) also contributes significantly to the rate acceleration. Interestingly, similar catalytic mechanisms in supramolecular chemistry, i.e., that take place via reduction of the entropic component of the free energy barrier, have previously been proposed in studies of the cycloaddition between azidoethylamine and propargylamine catalyzed by cucurbit[6]uril[22] and the Diels−Alder reaction between 9-anthracenemethanol and *N*-cyclohexylmaleimide catalyzed by cyclodextrins.[13]

DOI: 10.1021/jacs.7b09102
J. Am. Chem. Soc. 2017, 139, 15494−15503

To summarize, the overall lowering of the barrier in the presence of the capsule compared to the solution reaction (28.0−21.6 = 6.4 kcal/mol) can be roughly divided into three parts: (a) a reduction of the entropic component (3.3 kcal/mol), (b) a geometric destabilization of the reactant **1**·**2** complex by the capsule (2.4 kcal/mol), and (c) a slight stabilization of the transition state **4-TS** by interactions with the capsule (0.7 kcal/mol). This energy decomposition is schematically visualized in Figure 6.

Here, it is also interesting to compare the findings of the present study, made at an all-QM level of theory, with the findings of the previous computational study on the same reaction, made at the ONIOM(M06-2X/6-311G(d,p):PM6) level, without solvation or thermal effects.[23] The potential energy barrier calculated in the present study inside $\mathbf{3}_2$ (20.6 kcal/mol) is similar to the one calculated in ref 23 (23.3 kcal/mol). In the same work, the barrier was also calculated at the ONIOM(B3LYP/6-311G(d,p):PM6) level of theory which resulted in a barrier of 21.5 kcal/mol.[23] However, only the $(\mathbf{3}\text{-}C_{4v})_2$ complex was investigated in the previous study. It is interesting to note that this does not seem to have any significant effect on the reaction barrier toward formation of **4** inside the capsule. On the other hand, the free energy barrier for formation of **5** calculated in the current study (40.3 kcal/mol) is significantly higher than the potential energy barrier calculated in that study (32.4 kcal/mol), which is probably due to the different computational protocol and the new form of the capsule found here, which must get more distorted to host **5-TS**.

3.5. Sensitivity to Methodology. The computational methods adopted in the current study are discussed in the Computational Details section above. Since different methods can be used for every step of the calculations, in the current section the sensitivity of some key results will be assessed as a function of the choice of density functional (B3LYP-D3(BJ),[24−30] M06-2X-D3,[28,47] PBE0-D3(BJ)[28,29,48−50] or TPSS-D3(BJ)[28,29,51]), dispersion correction (DFT-D3(BJ),[28,29] XDM[52] or MBD@rsSCS[53−55]), basis set (6-311+G(2d,2p) or def2-TZVP,[56] with or without the parametrized counterpoise correction gCP[57]), solvation model (COSMO*therm*,[33,34] SMD[58] or C-PCM[59,60]), and finally the protocol for calculating the free energy (RRHO or quasi-RRHO[37]).

Although the full free energy profiles were calculated with all different computational schemes, for space reasons, only the effects on four specific free energies will be discussed here: First, the stability of the kite dimer $(\mathbf{3}\text{-}C_{2v})_2$ relative to **7**·**8**@$\mathbf{3}_2$, i.e., eq 1 above. Second, the stability of the Michaelis complex **1**·**2**@$\mathbf{3}_2$ relative to **2**·**2**@$\mathbf{3}_2$, i.e., the free energy calculated for eq 6, which according to experiments should be exergonic.[9]

$$\mathbf{2}\cdot\mathbf{2}@\mathbf{3}_2 + \mathbf{1} \rightleftharpoons \mathbf{1}\cdot\mathbf{2}@\mathbf{3}_2 + \mathbf{2} \quad (6)$$

Third, the change in cycloaddition barrier in the capsule compared to the outside reaction, denoted $\Delta(\Delta G^{\ddagger})_{acc}$. Last, the free energy associated with the catalyst regeneration, i.e., the free energy of eq 5. This can also be described as the increase of the free energy barrier in the second catalytic cycle compared to the first. The free energies calculated with different methodologies are presented in Table 3.

Overall, with a few exceptions discussed below, the results are stable under the variation of the methodology. The largest effect of the choice of methodology is observed for the relative stability of the kite dimer. The result that sticks out the most is obtained with the TPSS-D3(BJ) functional, which predicts the free energy of the separate **7**, **8** and kite dimer $(\mathbf{3}\text{-}C_{2v})_2$ to be −13.7 kcal/mol compared to **7**·**8**@$\mathbf{3}_2$. This is in disagreement with the multitude of signals observed in the NMR when **3** was mixed with distilled **6**.[41] If the TPSS-D3(BJ) prediction would be correct, the signal of the kite dimer would have dominated the ^{1}H NMR spectrum both in distilled and off-the-shelf **6**.

A technical note here concerns the solvation methods. In the creation of the solute cavities used by the implicit models tested here, it was found that two disjoint cavities were formed—one around the capsule atoms, and one around the encapsulated molecules. This means that some of the dielectric continuum that represents the solvent in these methods will actually be located between the capsule walls and the guest molecules. Hence, the encapsulated guest molecules will to some extent be treated as if they were interacting directly with the solvent, which is unphysical. To correct for this, in one approach the two cavities were joined by the addition of extra cavity spheres in the void between the host and the guests. The largest effect of this treatment is obtained for eq 1, which becomes 2−3 kcal/mol less endergonic when the cavities are joined.

To summarize this section, in spite of some variation in the calculated free energies, the overall trends are rather stable with respect to the choice of method. Namely, the kite dimer is

Table 3. Free Energies (kcal/mol) Calculated with Different Methods[a]

method	ΔG° (eq 1)[b]	ΔG° (eq 6)[c]	$\Delta(\Delta G^{\ddagger})_{acc}$[d]	ΔG° (eq 5)[e]
B3LYP-D3(BJ)/6-311+G(2d,2p), COSMO-RS, quasi-RRHO				
	+5.7	**+1.7**	**−6.4**	**+4.2**
Functionals				
M06-2X-D3	+11.0	+2.8	−4.0	+2.1
PBE0-D3(BJ)	+4.6	+1.2	−6.8	+5.6
TPSS-D3(BJ)	−13.7	+1.0	−7.8	+6.1
Dispersion model				
PBE0-XDM[f]	+4.9	+0.4	−7.8	+7.7
PBE0-MBD@rsSCS[f]	+8.2	0.0	−7.1	+6.2
Basis set				
def2-TZVP	+3.9	+1.7	−6.4	+4.1
def2-TZVP+gCP	+0.5	+0.7	−6.6	+4.7
Solvation model				
SMD	+7.2	+4.2	−8.7	+6.1
SMD (Joined cavities)[g]	+4.4	+3.6	−7.9	+4.8
C-PCM	+13.3	+1.6	−7.8	+6.4
C-PCM (Joined cavities)[g]	+11.0	+1.0	−9.6	+8.3
Free energy protocol				
RRHO	+3.0	+1.6	−3.8	+2.6
	+4.8[h]			
quasi-RRHO	+6.7[h]			

[a]All corrections except the one being varied is calculated using the procedure in the Computational Details section. When the functional is varied, only the energy at the 6-311+G(2d,2p) level is recalculated. [b]The free energy of $(\mathbf{3}\text{-}C_{2v})_2$ with respect to **7**·**8**@$\mathbf{3}_2$, i.e., eq 1. Unless stated otherwise, one imaginary frequency of 10*i* cm^{-1} is treated as real in the entropy calculations. [c]The free energy of **1**·**2**@$\mathbf{3}_2$ relative to **2**·**2**@$\mathbf{3}_2$, i.e., eq 6. [d]The difference in the barrier for cycloaddition inside compared to outside the capsule. [e]The free energy of the catalyst regeneration process, i.e., eq 5. [f]The densities used by the wave function-based dispersion corrections are calculated at the 6-31+G(d,p) level of theory. [g]The cavities of capsule and guests are joined together by filling the void between them using the ExtraSph keyword in the Gaussian 09 software. [h]One imaginary frequency of 10*i* cm^{-1} is discarded in the entropy calculations.

DOI: 10.1021/jacs.7b09102
J. Am. Chem. Soc. 2017, 139, 15494−15503

calculated to be unstable with respect to $7{\cdot}8@3_2$, complex $2{\cdot}2@3_2$ is calculated to be more stable than $1{\cdot}2@3_2$, the capsule is predicted to lower the barrier for cycloaddition compared to the uncatalyzed reaction, and the barrier is calculated to be higher in the second cycle compared to the first.

4. CONCLUSIONS

The present computational study has been concerned with the elucidation of the factors causing the acceleration of the cycloaddition reaction between phenyl acetylene and phenyl azide inside a self-assembled capsule host, 3_2. First, the capsule was characterized structurally and a new C_4-symmetric structure of the **3** monomer in the 3_2 complex was identified. This structure is significantly more stable than the previously proposed $(\mathbf{3}\text{-}C_{4v})_2$ structure. Notably, inclusion of the dispersion correction in the calculations was shown to be crucial for this discovery.

The binding free energies of various guest compounds, including the reactants, the solvent, and solvent impurities, were next calculated and reproduced quite well the experimental trends. Here, explicit consideration of the experimental concentrations of the guests was shown to yield generally better agreement with the experiments.

Very importantly, the accelerating effect of the capsule on the reaction rate was well reproduced by the calculations. Namely, a free energy barrier of 21.6 kcal/mol was obtained inside the capsule, as compared to 28.0 kcal/mol outside. Also, the exclusive production of the 1,4-regioisomer of the product is well reproduced.

The geometries and energies were analyzed in detail and the main source of the rate acceleration in the presence of 3_2 could be identified. The reduction of the entropic penalty associated with the bringing together of reactants **1** and **2** to form the reactant supercomplex **1·2** could be estimated to 3.4 kcal/mol, while the destabilization of the encapsulated **1·2** complex due to the geometric constraints imposed by the host was estimated to contribute by 2.3 kcal/mol to the barrier lowering. On the other hand, the relative stabilization provided by the host 3_2 of the transition state compared to the reactants amounted only to 0.7 kcal/mol.

Finally, the sensitivity of the results to the adopted computational protocol was examined by varying the involved components, such as the density functional, basis set, solvation model, dispersion correction, and method for calculating the free energy correction. With a few exceptions the calculations show that the conclusions are quite stable.

The level of insight generated by the calculations is a testament to usefulness of the all-QM approach adopted in the current study.

■ ASSOCIATED CONTENT

Supporting Information

The Supporting Information is available free of charge on the ACS Publications website at DOI: 10.1021/jacs.7b09102.

Optimized geometries of all host–guest complexes in Table 1 and 2, details of the volume calculations, and absolute energies and Cartesian coordinates for all species (PDF)

■ AUTHOR INFORMATION

Corresponding Author

*fahmi.himo@su.se

ORCID

Jeremy N. Harvey: 0000-0002-1728-1596

Fahmi Himo: 0000-0002-1012-5611

Notes

The authors declare no competing financial interest.

■ ACKNOWLEDGMENTS

FH acknowledges financial support from the Swedish Research Council, the Knut and Alice Wallenberg Foundation and the Göran Gustafsson Foundation. JR is grateful to the National Science Foundation (CHE 1506266) for support.

■ REFERENCES

(1) Rebek, J., Jr. *Angew. Chem., Int. Ed.* **2005**, *44*, 2068–2078.
(2) Fiedler, D.; Leung, D. H.; Bergman, R. G.; Raymond, K. N. *Acc. Chem. Res.* **2005**, *38*, 351–360.
(3) Yoshizawa, M.; Klosterman, J. K.; Fujita, M. *Angew. Chem., Int. Ed.* **2009**, *48*, 3418–3438.
(4) Wiester, M. J.; Ulmann, P. A.; Mirkin, C. A. *Angew. Chem., Int. Ed.* **2011**, *50*, 114–137.
(5) Dong, Z.; Luo, Q.; Liu. *Chem. Soc. Rev.* **2012**, *41*, 7890–7908.
(6) Hooley, R. J.; Rebek, J., Jr. *Chem. Biol.* **2009**, *3*, 255–264.
(7) Raynal, M.; Ballester, P.; Vidal-Ferran, A.; van Leeuwen, P. W. N. M. *Chem. Soc. Rev.* **2014**, *43*, 1734–1787.
(8) Deraedt, C.; Astruc, D. *Coord. Chem. Rev.* **2016**, *324*, 106–122.
(9) Chen, J.; Rebek, J., Jr. *Org. Lett.* **2002**, *4*, 327–329.
(10) Antony, J.; Sure, R.; Grimme, S. *Chem. Commun.* **2015**, *51*, 1764–1774.
(11) Alvira, E.; Cativiela, C.; García, J. I.; Mayoral, J. A. *Tetrahedron Lett.* **1995**, *36*, 2129–2132.
(12) Kim, S. P.; Leach, A. G.; Houk, K. N. *J. Org. Chem.* **2002**, *67*, 4250–4260.
(13) Chen, W.; Sun, L.; Tang, Z.; Chang, C.-E. *bioRxiv* **2017**, 169565.
(14) Xu, L.; Hua, W.; Hua, S.; Li, J.; Li, S. *J. Org. Chem.* **2013**, *78*, 3577–3582.
(15) Furuki, T.; Hosokawa, F.; Sakurai, M.; Inoue, Y.; Chûjô, R. *J. Am. Chem. Soc.* **1993**, *115*, 2903–2911.
(16) Luzhkov, V.; Åqvist, J. *Chem. Phys. Lett.* **1999**, *302*, 267–272.
(17) Karnes, J. J.; Benjamin, I. *J. Phys. Chem. C* **2017**, *121*, 19209–19217.
(18) Fruschicheva, M. P.; Mukherjee, S.; Warshel, A. *J. Phys. Chem. B* **2012**, *116*, 13353–13360.
(19) Ootani, Y.; Akinaga, Y.; Nakajima, T. *J. Comput. Chem.* **2015**, *36*, 459–466.
(20) Cacciapaglia, R.; Di Stefano, S.; Mandolini, L. *Acc. Chem. Res.* **2004**, *37*, 113–122.
(21) Carlqvist, P.; Maseras, F. *Chem. Commun.* **2007**, 748–750.
(22) Goehry, C.; Besora, M.; Maseras, F. *ACS Catal.* **2015**, *5*, 2445–2451.
(23) Cantillo, D.; Ávalos, M.; Babiano, R.; Cintas, P.; Jiménez, J. L.; Palacios, J. *Org. Biomol. Chem.* **2011**, *9*, 7638–7642.
(24) Becke, A. D. *J. Chem. Phys.* **1993**, *98*, 5648–52.
(25) Becke, A. D. *Phys. Rev. A: At., Mol., Opt. Phys.* **1988**, *38*, 3098–3100.
(26) Lee, C.; Yang, W.; Parr, R. G. *Phys. Rev. B: Condens. Matter Mater. Phys.* **1988**, *37*, 785–789.
(27) Stephens, P. J.; Devlin, F. J.; Chabalowski, C. F.; Frisch, M. J. *J. Phys. Chem.* **1994**, *98*, 11623–11627.
(28) Grimme, S.; Antony, J.; Ehrlich, S.; Krieg, H. *J. Chem. Phys.* **2010**, *132*, 154104–22.
(29) Grimme, S.; Ehrlich, S.; Goerigk, L. *J. Comput. Chem.* **2011**, *32*, 1456–1465.
(30) Becke, A. D.; Johnson, E. R. *J. Chem. Phys.* **2005**, *123*, 154101.
(31) Frisch, M. J.; Trucks, G. W.; Schlegel, H. B.; Scuseria, G. E.; Robb, M. A.; Cheeseman, J. R.; Scalmani, G.; Barone, V.; Mennucci, B.; Petersson, G. A.; Nakatsuji, H.; Caricato, M.; Li, X.; Hratchian, H.

DOI: 10.1021/jacs.7b09102
J. Am. Chem. Soc. 2017, 139, 15494–15503

P.; Izmaylov, A. F.; Bloino, J.; Zheng, G.; Sonnenberg, J. L.; Hada, M.; Ehara, M.; Toyota, K.; Fukuda, R.; Hasegawa, J.; Ishida, M.; Nakajima, T.; Honda, Y.; Kitao, O.; Nakai, H.; Vreven, T.; Montgomery, J. A., Jr.; Peralta, J. E.; Ogliaro, F.; Bearpark, M.; Heyd, J. J.; Brothers, E.; Kudin, K. N.; Staroverov, V. N.; Keith, T.; Kobayashi, R.; Normand, J.; Raghavachari, K.; Rendell, A.; Burant, J. C.; Iyengar, S. S.; Tomasi, J.; Cossi, M.; Rega, N.; Millam, J. M.; Klene, M.; Knox, J. E.; Cross, J. B.; Bakken, V.; Adamo, C.; Jaramillo, J.; Gomperts, R.; Stratmann, R. E.; Yazyev, O.; Austin, A. J.; Cammi, R.; Pomelli, C.; Ochterski, J. W.; Martin, R. L.; Morokuma, K.; Zakrzewski, V. G.; Voth, G. A.; Salvador, P.; Dannenberg, J. J.; Dapprich, S.; Daniels, A. D.; Farkas, O.; Foresman, J. B.; Ortiz, J. V.; Cioslowski, J.; Fox, D. J. *Gaussian 09*, Revision D.01; Gaussian, Inc.: Wallingford, CT, 2013.

(32) Karton, A.; Goerigk, L. *J. Comput. Chem.* **2015**, *36*, 622−632.

(33) *COSMOtherm, C3.0*, release 1601, revision 2587; COSMOlogic GmbH & Co KG.

(34) Eckert, F.; Klamt, A. *AIChE J.* **2002**, *48*, 369−385.

(35) Perdew, J. P. *Phys. Rev. B: Condens. Matter Mater. Phys.* **1986**, *33*, 8822−8824.

(36) Schaefer, A.; Huber, C.; Ahlrichs, R. *J. Chem. Phys.* **1994**, *100*, 5829−5835.

(37) Grimme, S. *Chem. - Eur. J.* **2012**, *18*, 9955−9964.

(38) Mecozzi, S.; Rebek, J., Jr. *Chem. - Eur. J.* **1998**, *4*, 1016−1022.

(39) Kleywegt, G. J.; Jones, T. A. *Acta Crystallogr., Sect. D: Biol. Crystallogr.* **1994**, *50*, 178−185.

(40) Bondi, A. J. *J. Phys. Chem.* **1964**, *68*, 441−451.

(41) Heinz, T.; Rudkevich, D. M.; Rebek, J., Jr. *Nature* **1998**, *394*, 764−766.

(42) The complex with C_{4v}-symmetric cavitands contains several low imaginary frequencies. Hence, the number of vibrational modes taken into account in the RRHO calculations are fewer and the free energies of the complexes are not comparable. Instead, the energy difference between the complexes with cavitands of C_4 and C_{4v} symmetries are calculated at the 6-311+G(2d,2p) level of theory, including solvation and 3-body dispersion effects.

(43) Moran, J. R.; Ericson, J. L.; Dalcanale, E.; Bryant, J. A.; Knobler, C. B.; Cram, D. J. *J. Am. Chem. Soc.* **1991**, *113*, 5707−5714.

(44) Körner, S. K.; Tucci, F. C.; Rudkevich, D. M.; Heinz, T.; Rebek, J., Jr. *Chem. - Eur. J.* **2000**, *6*, 187−195.

(45) Li, X.-B.; Song, Q.-H. *Heteroat. Chem.* **2007**, *18*, 203−207.

(46) Craig, S. L.; Lin, S.; Chen, J.; Rebek, J., Jr. *J. Am. Chem. Soc.* **2002**, *124*, 8780−8781.

(47) Zhao, Y.; Truhlar, D. G. *Theor. Chem. Acc.* **2008**, *120*, 215−241.

(48) Perdew, J. P.; Burke, K.; Ernzerhof, M. *Phys. Rev. Lett.* **1996**, *77*, 3865−3868.

(49) Perdew, J. P.; Burke, K.; Ernzerhof, M. *Phys. Rev. Lett.* **1997**, *78*, 1396.

(50) Adamo, C.; Berone, V. *J. Chem. Phys.* **1999**, *110*, 6158−6169.

(51) Tao, J. M.; Perdew, J. P.; Staroverov, V. N.; Scuseria, G. E. *Phys. Rev. Lett.* **2003**, *91*, 146401.

(52) Becke, A. D.; Johnson, E. R. *J. Chem. Phys.* **2007**, *127*, 154108.

(53) Tkatchenko, A.; Scheffler, M. *Phys. Rev. Lett.* **2009**, *102*, 073005.

(54) Tkatchenko, A.; DiStasio, R. A., Jr.; Car, R.; Scheffler, M. *Phys. Rev. Lett.* **2012**, *108*, 236402.

(55) Ambrosetti, A.; Reilly, A. M.; DiStasio, R. A., Jr.; Tkatchenko, A. *J. Chem. Phys.* **2014**, *140*, 18A508.

(56) Weigend, F.; Ahlrichs, R. *Phys. Chem. Chem. Phys.* **2005**, *7*, 3297−3305.

(57) Kruse, H.; Grimme, S. *J. Chem. Phys.* **2012**, *136*, 154101.

(58) Marenich, A. V.; Cramer, C. J.; Truhlar, D. G. *J. Phys. Chem. B* **2009**, *113*, 6378−6396.

(59) Barone, V.; Cossi, M. *J. Phys. Chem. A* **1998**, *102*, 1995−2001.

(60) Cossi, M.; Rega, N.; Scalmani, G.; Barone, V. *J. Comput. Chem.* **2003**, *24*, 669−681.

DOI: 10.1021/jacs.7b09102
J. Am. Chem. Soc. 2017, 139, 15494−15503